PNAS
www.pnas.org

Supplementary Information for

Implantable Multi-reservoir Device with Stimulus-responsive Membrane for On-demand and Pulsatile Delivery of Growth Hormone

Seung Ho Lee[+], Huiyan Piao[+], Yong Chan Cho, Se-Na Kim, Goeun Choi, Cho Rim Kim, Han Bi Ji, Chun Gown Park, Cheol Lee, Chong In Shin, Won-Gun Koh, Young Bin Choy[*], Jin-Ho Choy[*]

Young Bin Choy, Jin-Ho Choy
Email: ybchoy@snu.ac.kr; jhchoy@dankook.ac.kr

This PDF file includes:

Figs. S1 to S10
Tables S1
Caption for Movie S1
References for SI reference citations

Other supplementary materials for this manuscript include the following:

Movie S1

www.pnas.org/cgi/doi/10.1073/pnas.1906931116

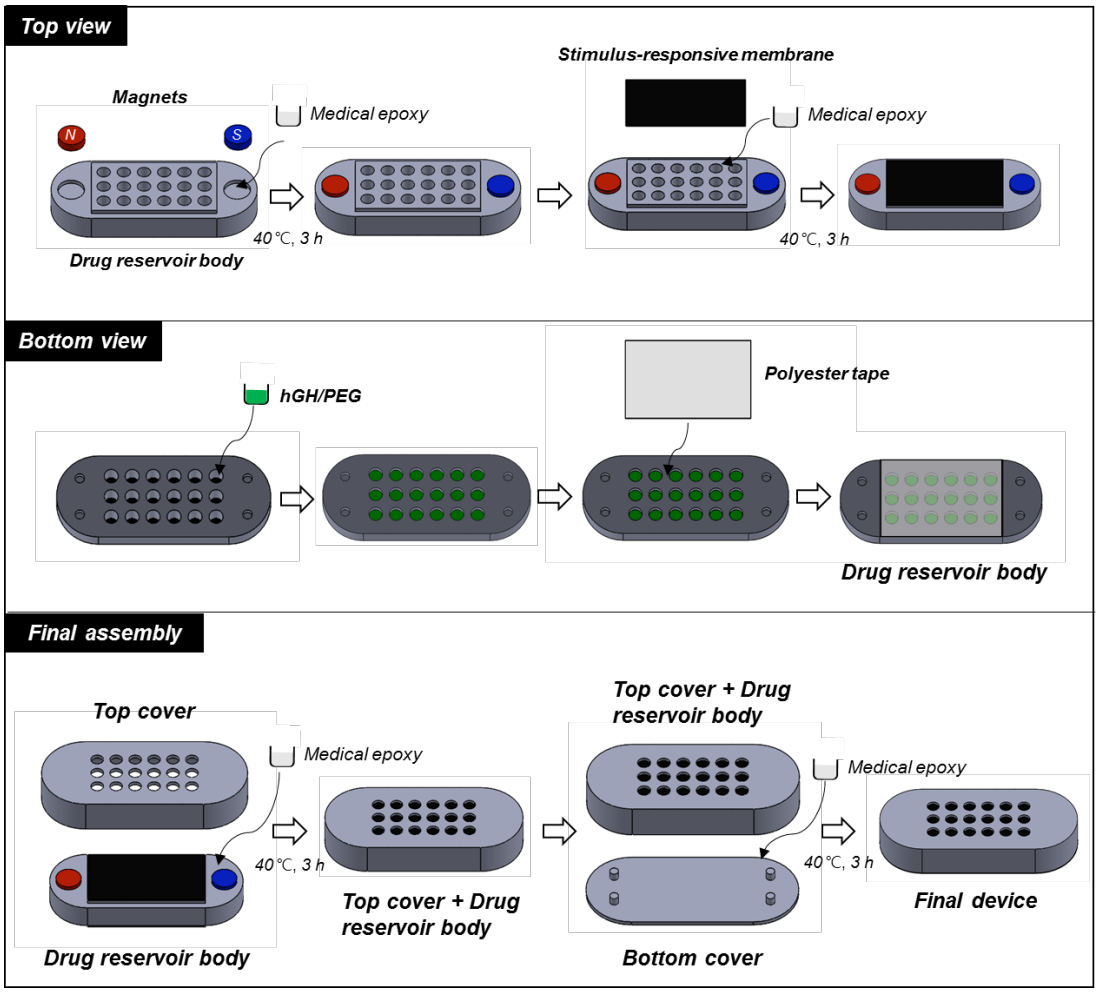

Fig. S1. Detailed description of the device fabrication procedures.

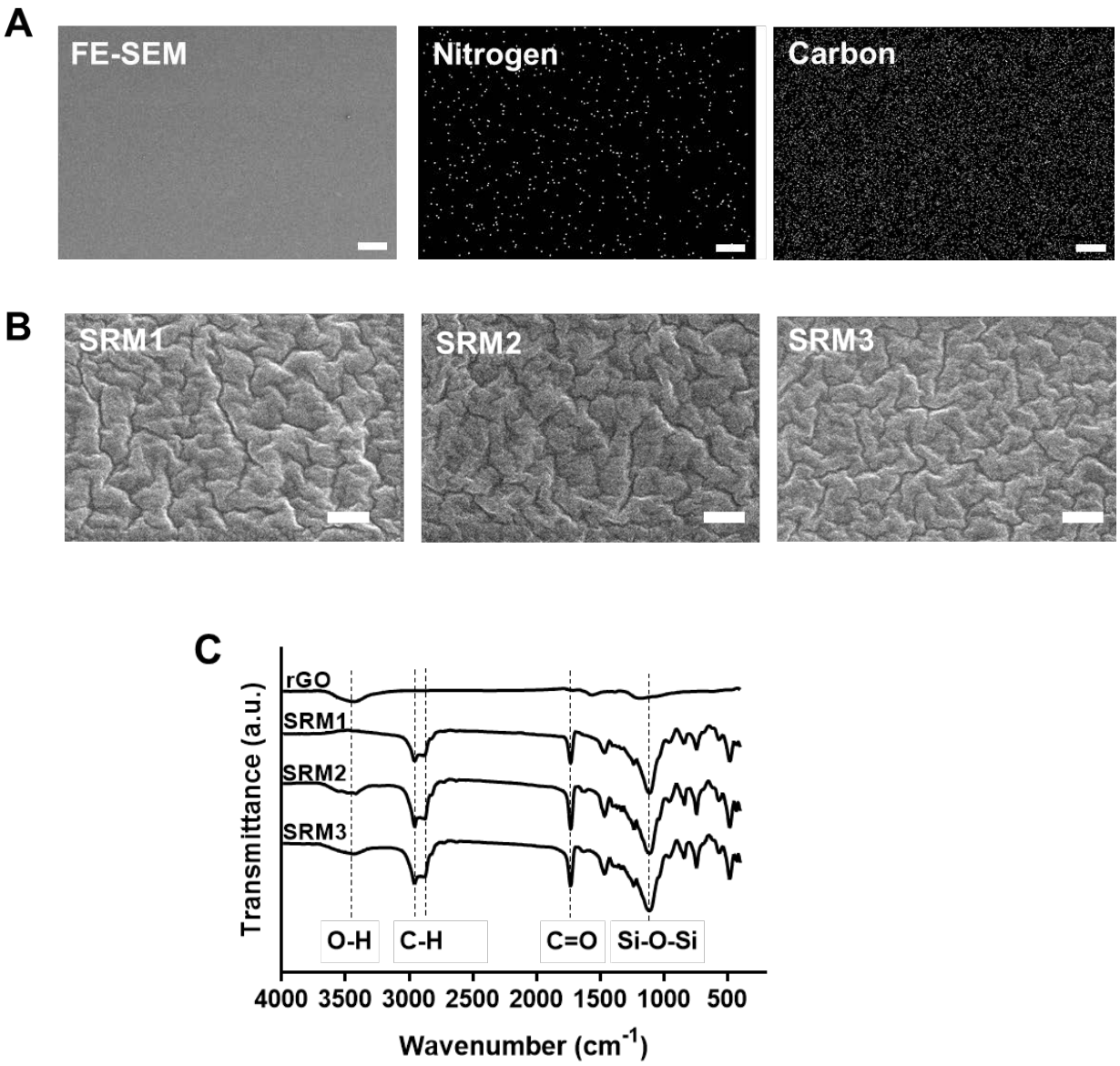
A
FE-SEM
Nitrogen
Carbon
B
SRM1
SRM2
SRM3
C
rGO
SRM1
SRM2
SRM3
Transmittance (a.u.)
O-H
C-H
C=O
Si-O-Si
4000 3500 3000 2500 2000 1500 1000 500
Wavenumber (cm-1)

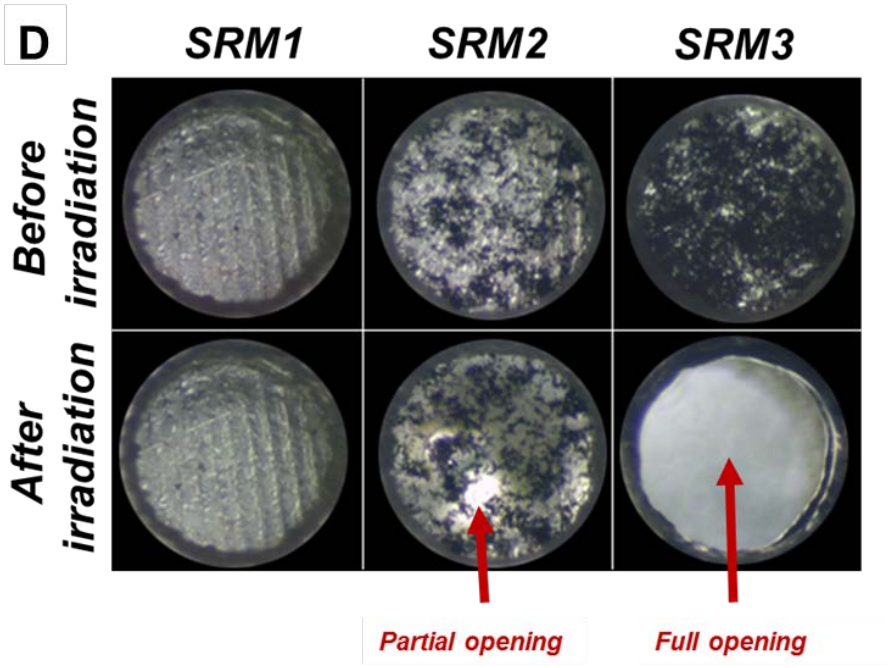

Fig. S2. Additional characterization of the SRMs. (**A**) FE-SEM image and its corresponding elemental mapping images of the SRM3 embedded with the nitrogen-doped rGO (NrGO) nanoparticles. Scale bars are 10 μm. To gain insight into the distribution profile of the rGO nanoparticles, we prepared the SRM3 under the same condition using NrGO nanoparticles instead, where the particle distribution could be imaged through elemental mapping analysis by detecting nitrogen. The NrGO nanoparticles were synthesized by the hydrothermal method with GO as raw material and urea as reducing-doping agent, following the previously reported protocol *(1)*. The microscopic image revealed that the NrGO nanoparticles were homogeneously distributed in the SRM3. (**B**) FE-SEM images of the SRMs. Scale bars are 500 nm. (**C**) FT-IR spectra of the SRMs. For the rGO nanoparticles, the characteristic peak observed at 3400 cm^{-1} corresponded to O-H stretching vibration. The SRM1 without the rGO nanoparticles showed the characteristic peaks at 2925 cm^{-1} and 2869 cm^{-1} due to C-H stretching, and those at 1730 cm^{-1} and 1120 cm^{-1} were ascribed to C=O carbonyl groups and Si-O-Si stretching, respectively. The SRM2 and SRM3 displayed all characteristic peaks originating from both SRM1 and rGO (2-*4*). (**D**) Optical images of the SRMs attached to a drug reservoir. The SRM3 only could be properly ruptured to fully open the drug reservoir after NIR irradiation.

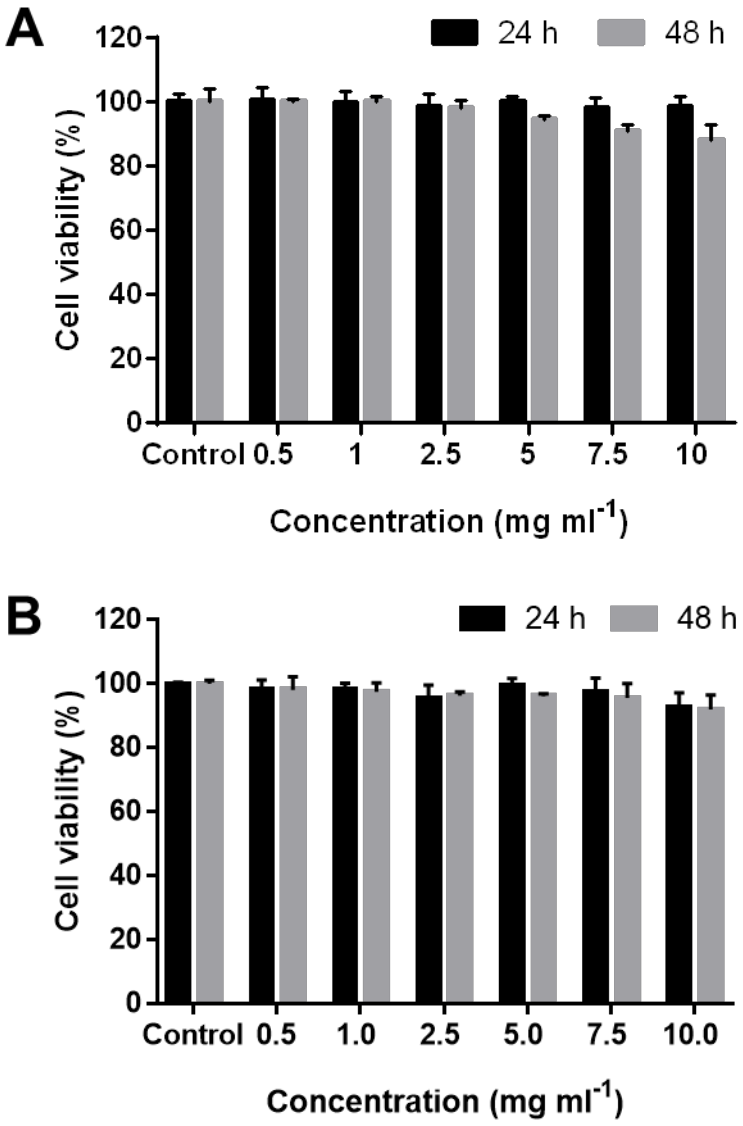

Fig. S3. *In-vitro* cytotoxicity analysis of the SRM3. Following the protocol described in the ISO10993-5 standard test method. **(A)** SRM3 without treatment **(B)** SRM3 immediately after NIR irradiation at an intensity of 8.85 W cm^{-1} for 5 s. For this test, the SRM3 without treatment or immediately after NIR irradiation was incubated in cell culture medium (RPMI 1640, Gibco, USA) at a concentration of 10 mg ml^{-1} for 72 h. Then, the medium was extracted and subsequently diluted to obtain media of varying concentrations. The resulting media were each added to a well with L929 cells, which were then incubated at 37 °C and 5% CO_2 for 24 h or 48 h. The cell viability was then assessed by MTT assay following the manufacturer's instructions (Sigma-Aldrich, USA). For all tested media, the cell viability was over 90%, suggesting that the SRM3 itself, as well as the SRM3 ruptured by NIR irradiation, did not generate any cytotoxic compounds. The experiments were performed in triplicate. Error bars are s.d.

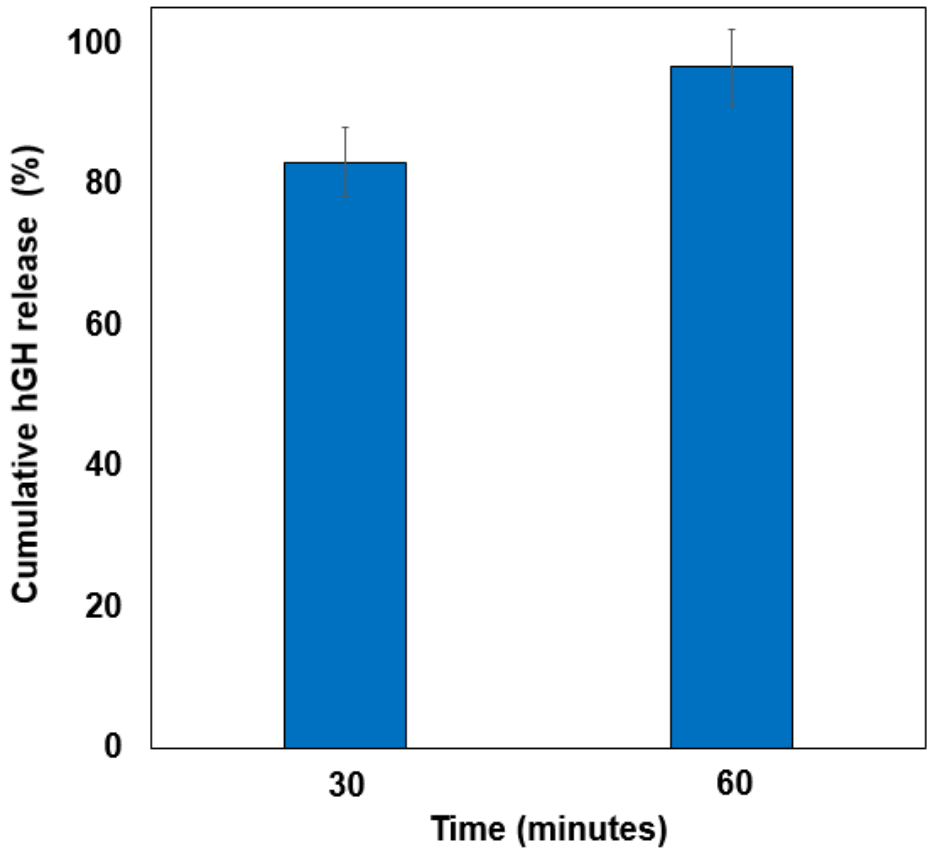

Fig. S4. ***In-vitro*** **hGH release profile at shorter time scales.** For this experiment, the device was irradiated with NIR light while being fully immersed in phosphate-buffered saline (PBS; pH 7.4) at 37 °C. The experiments were performed in triplicate. Error bars are s.d.

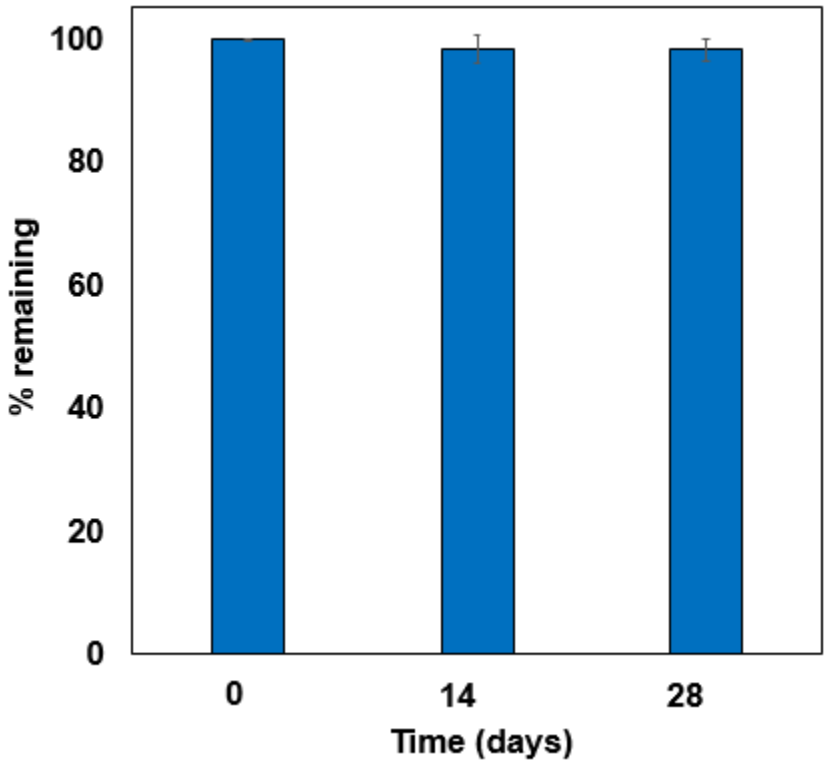

Fig. S5. Stability evaluation of hGH. The device loaded with hGH was incubated at 37 °C for 0, 14 or 28 days. After each incubation period, the drug reservoir was opened and the hGH was extracted and dissolved in pH 7.4 PBS, which was analysed by reversed-phase high-performance liquid chromatography (RP-HPLC, Agilent 1260 series, Agilent Technologies, USA), as described in Methods in the main text. The results suggest that the hGH in the device was stable for 28 days at body temperature.

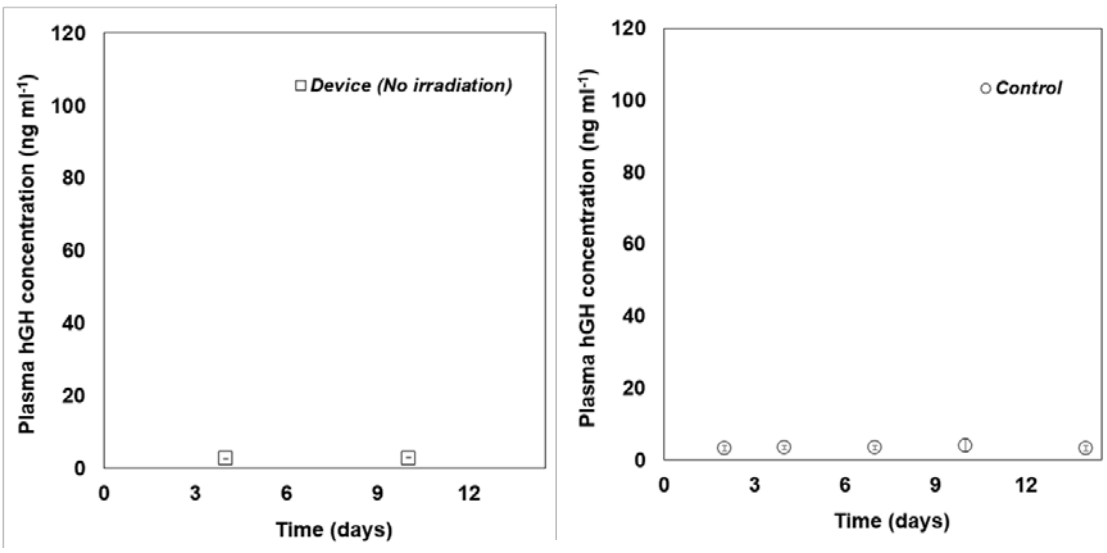

Fig. S6. ***In-vivo*** **leak test results of the device.** The plasma hGH concentration in the device group (n = 4) was measured immediately before NIR irradiation, which was compared to that of the control group (n = 4). Error bars are s.d.

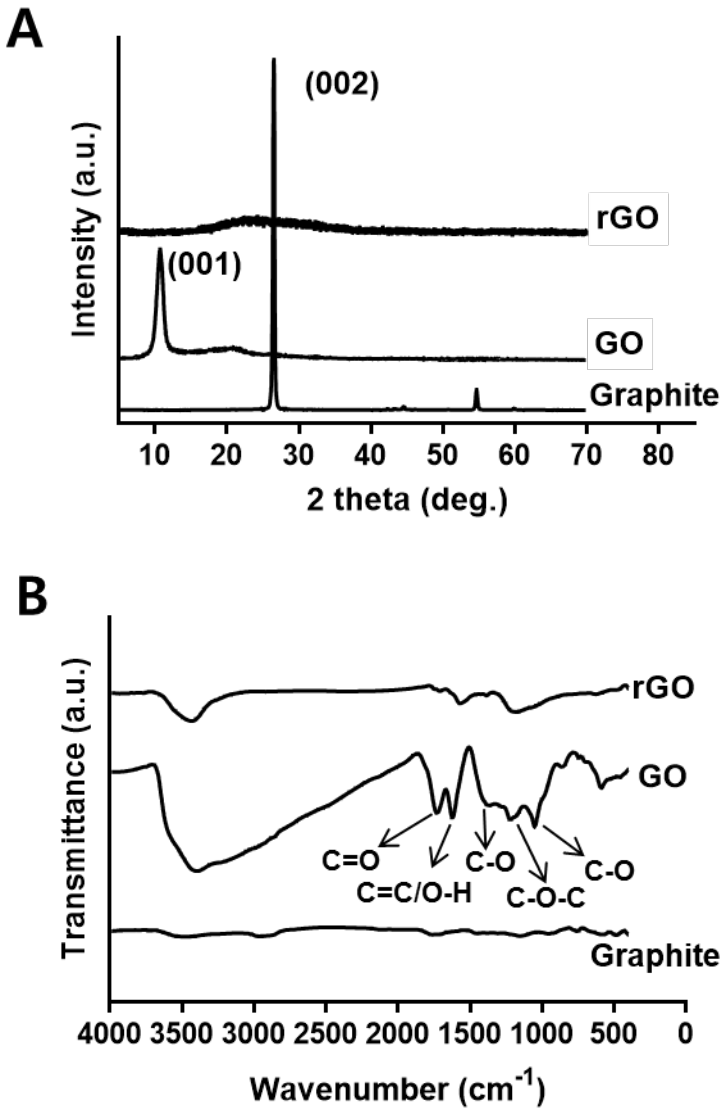
A
(002)
(001)
rGO
GO
Graphite
Intensity (a.u.)
10 20 30 40 50 60 70 80
2 theta (deg.)
B
rGO
GO
C=O
C=C/O-H
C-O
C-O-C
C-O
Graphite
Transmittance (a.u.)
4000 3500 3000 2500 2000 1500 1000 500 0
Wavenumber (cm-1)

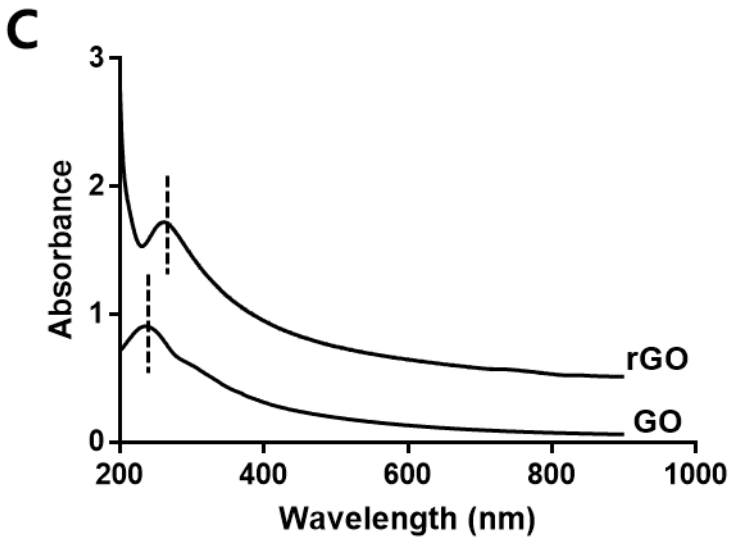
C
Absorbance
Wavelength (nm)
rGO
GO
0
1
2
3
200
400
600
800
1000

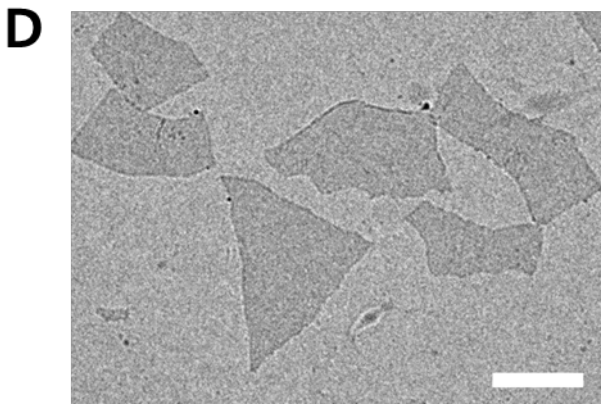
D

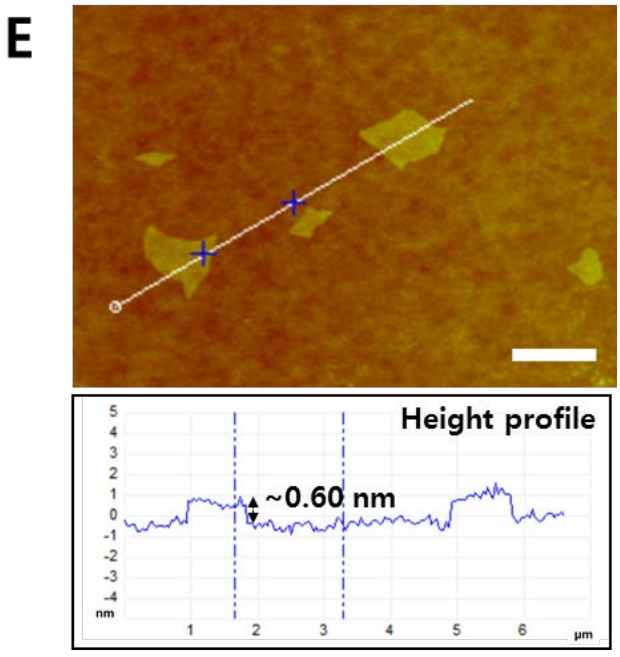
E
Height profile
~0.60 nm
nm
µm

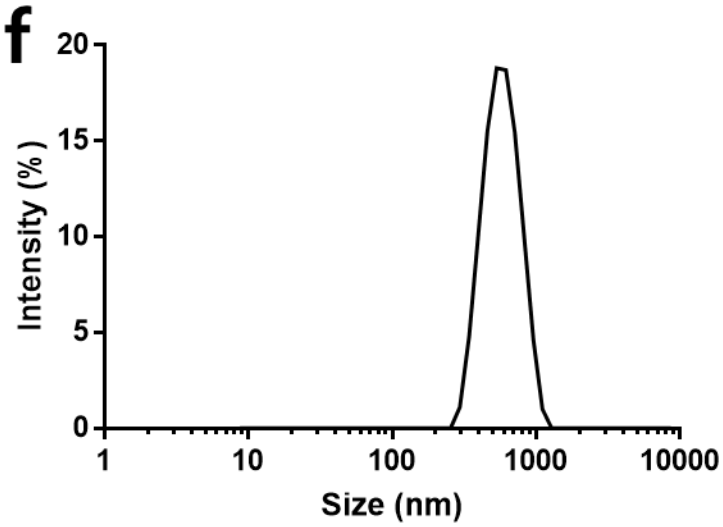
f
Intensity (%)
20
15
10
5
0
1
10
100
1000
10000
Size (nm)

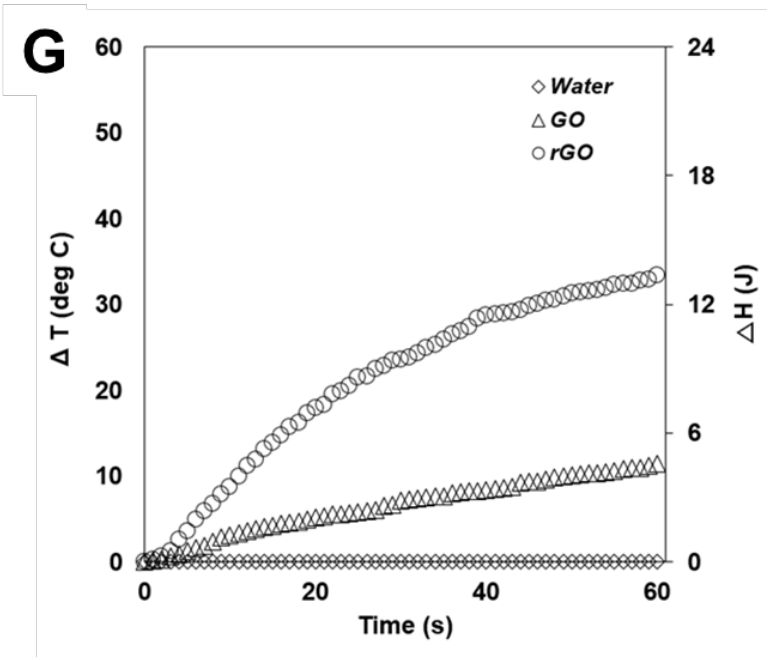
G
Water
GO
rGO
Δ T (deg C)
△H (J)
60
50
40
30
20
10
0
24
18
12
6
0
0
20
40
60
Time (s)

Fig. S7. Characterizations of rGO, GO and graphite at each reaction step. (**A**) XRD patterns: graphite exhibited a strong basal reflection (002) peak with a d-spacing of approximately 0.34 nm. Upon oxidation, the diffraction peak (001) of GO appeared at a lower 2 theta angle with a d-spacing of 0.81 nm due to the introduction of a number of oxygen-containing groups on the edges and surfaces of each layer. After reduction, no apparent diffraction peak was detected, indicating the formation of rGO. (**B**) FT-IR spectra: the spectral peak intensities of the rGO, corresponding to the oxygen-containing groups and hydroxyl groups, were significantly reduced compared to those of the GO, confirming the reduction of GO to form rGO. (**C**) UV-visible spectra (JASCO V-630, JASCO, Japan) obtained from the GO and rGO suspensions (0.1 mg ml^{-1}): the rGO exhibited an enhancement of NIR absorption region with the peak at 270 nm, which was red-shifted from 230 nm of GO. Those results indicated that the electronic coupling within the sheet of rGO nanoparticles could be revived upon reduction of GO**.** (**D**) TEM image showing the monolayer rGO nanoparticles. The scale bar represents 500 nm. (**E**) AFM image of the rGO nanoparticles with the corresponding height profile measured along the white line in the image. The scale bar represents 1 μm. The image was obtained by a typical tapping mode (Veeco Dimension 3100, Digital Instrument, USA) with the rGO nanoparticles deposited on a silicon wafer substrate by spin-coating. The height of the rGO was measured to be approximately 0.60 nm, which was larger than the calculated value of a single layer of graphene (0.34 nm) but smaller than that of its double layers (0.68 nm) due to the remaining oxygen-containing groups on the edges and surfaces of rGO sheets *(4)*. (**F**) Particle size distribution of rGO: The average particle size was approximately 600 nm (Nano ZS, Malvern, UK), which was similar to that observed in the TEM image. All the results above suggest that the monolayer rGO nanoparticles were successfully prepared in this work (*5*, *6*). (**G**) Photothermal properties of water and aqueous suspensions of GO and rGO (0.1 mg ml^{-1}). The temperature was recorded (Optris LaserSight, Optris, Germany) during NIR irradiation (808 nm, 8.85 W cm^{-2}) upon 0.5 mL of each sample for 60 s. With the same dose of NIR irradiation, the rGO exhibited the most dramatic increase in temperature.

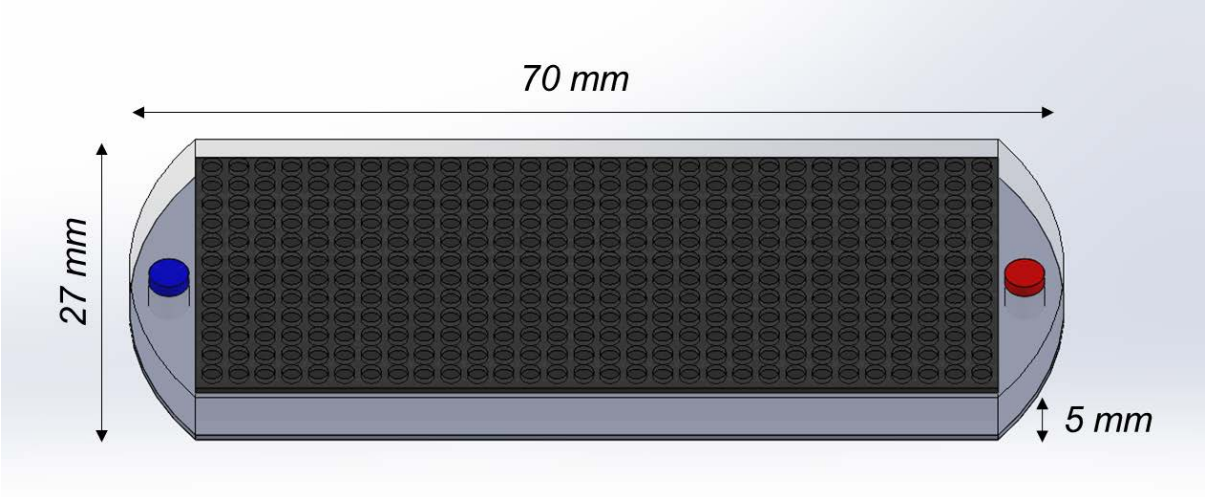

Fig. S8. Schematic of the exemplary device envisioned with clinical applications. The device can be designed to contain 360 drug reservoirs, giving dimensions of 70 mm x 27 mm x 5 mm (*l* x *w* x *h*) with a volume of approximately 9.5 ml.

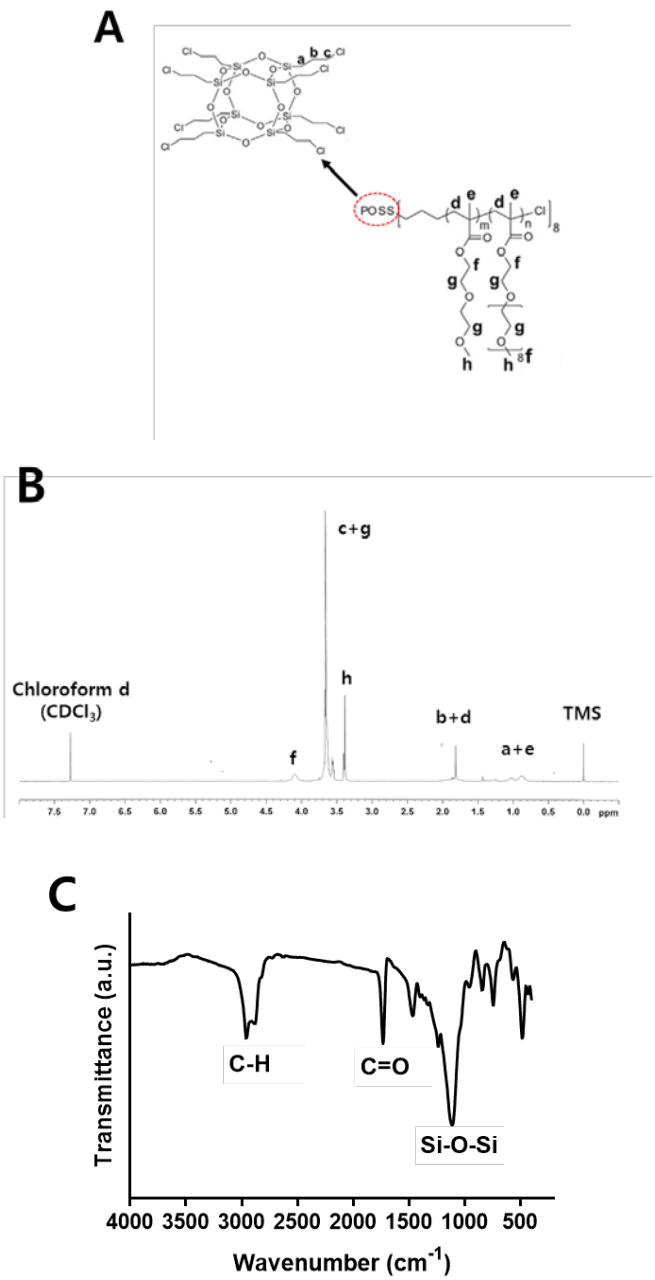

Fig. S9. Characterization of POSS(MEO$_2$MA-co-OEGMA). (**A**) Drawing of the chemical structure. (**B**) ^{1}H NMR spectra. The resonances at 0.8–1.1 ppm (a+e: $CH_2C(CH_3)$), 1.7–2.0 ppm (b+d: $CH_2C(CH_3)$), 3.4 ppm (h: $CH_2CH_2OCH_3$), 3.5–3.7 ppm (c+g: CH_2CH_2O) and 4.1 ppm (f: CH_2CH_2O) were the characteristic signals of the protons at different positions observed with the POSS(MEO$_2$MA-co-OEGMA). (**C**) FT-IR spectra. The peaks at 2925 cm^{-1} and 2869 cm^{-1} were ascribed to C-H stretching. The strong peaks observed at 1730 cm^{-1} and 1120 cm^{-1} could be attributed to the C=O carbonyl groups and Si-O-Si stretching, respectively. The results from the ^{1}H NMR and FT-IR analyses confirmed successful fabrication of the POSS(MEO$_2$MA-co-OEGMA) in this work *(3)*.

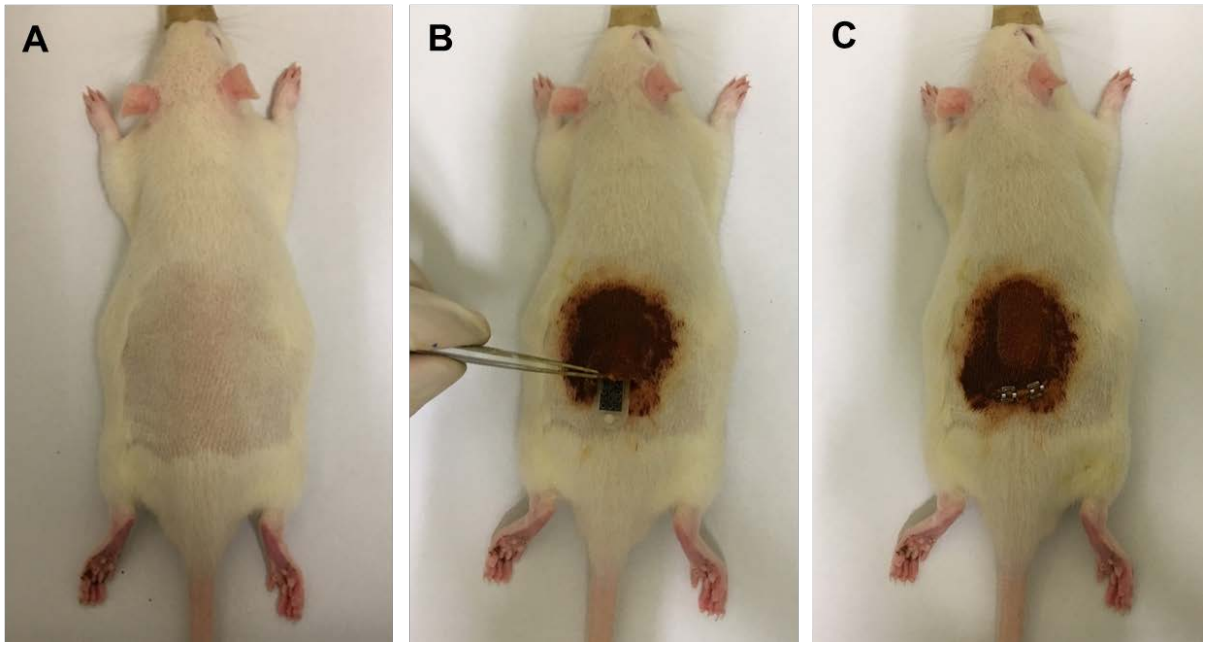

Fig. S10. Surgical procedure for device implantation. (**A**) A hypophysectomized rat was anaesthetized by isoflurane, and the dorsal area was shaved. (**B**) After the area was sterilized with betadine, a skin incision (1-2 cm) was made, and the device was implanted into the subcutaneous pocket. (**C**) The wound was closed with surgical clips (9 mm autoclips, Clay Adams, USA) and disinfected with betadine.

Table S1. Inflammatory markers in blood plasma.
Inflammatory markers in plasma, such as IL-1b, IL-6 and TNF-α, were measured at the end point of *in-vivo* experiments. For all animals in the device group (n = 4), abnormal elevation of inflammatory markers was not observed (*7*), and their levels in plasma were not different from those in the control group without device implantation (n = 4).

	IL-1b (pg ml^{-1})	**IL-6 (pg ml^{-1})**	**TNF-α (pg ml^{-1})**
Device group	102 ± 9	71 ± 6	55 ± 3
Control group	108 ± 5	69 ± 4	57 ± 6

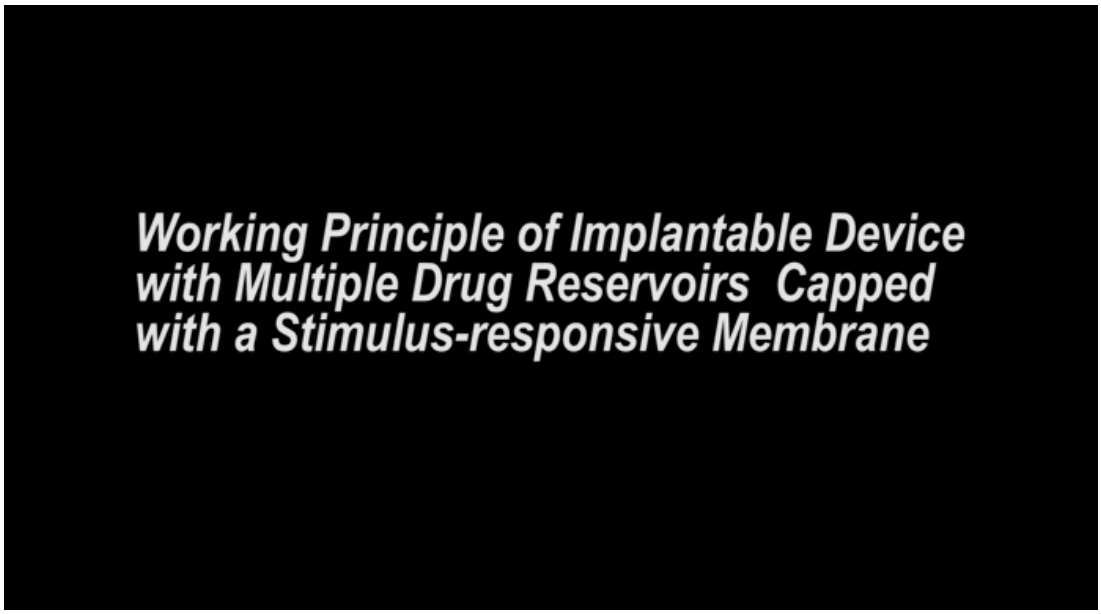

Movie S1. Working principle of the device.

References

1. Guo HL, Su P, Kang X, Ning SK (2013) Synthesis and characterization of nitrogen-doped graphene hydrogels by hydrothermal route with urea as reducing-doping agents. *J Mater Chem A* 1: 2248-2255.
2. Shi Y, Xiong D, Li J, Wang K, Wang N (2017) In situ repair of graphene defects and enhancement of its reinforcement effect in polyvinyl alcohol hydrogels. *RSC Adv* 7: 1045.
3. Yuan W, Shen T, Liu X, Ren J (2013) Star-shapedinorganic–organic hybridpolymerswithpolyhedral oligomericsilsesquioxanecore:Synthesis,self-assembly and tunablethermoresponse. *Mater Lett* 111: 9–12.
4. Novoselov KS, et al. (2004) Electric Field Effect in Atomically Thin Carbon Films. *Science* 306: 666 .
5. Zhou Q, et al. (2015) Preparation of a reduced graphene oxide/zirconia nanocomposite and its application as a novel lubricant oil additive. *RSC Adv* 5: 91802-91812.
6. McAllister MJ, et al. (2007) Sheet Functionalized Graphene by Oxidation and Thermal Expansion of Graphite. *Chem Mater* 19: 4396–4404.
7. Wang X, Lennartz MR, Loegering DJ, Stenken JA (2007) Interleukin-6 collection through long-term implanted microdialysis sampling probes in rat subcutaneous space. *Anal Chem* 79: 1816-1824.